



ELSEVIER

Ultramicroscopy 84 (2000) 57–64

ultramicroscopy

www.elsevier.nl/locate/ultramic

# Defocus-gradient corrected back-projection

Grant J. Jensen, Roger D. Kornberg\*

*Department of Structural Biology, Stanford University, School of Medicine, Stanford, CA 94305, USA*

Received 2 September 1999; received in revised form 20 December 1999

## Abstract

Three-dimensional reconstructions of icosahedral viruses from cryoelectron microscope images have reached resolutions where the microscope depth of field is a significant resolution-limiting factor. An analytical treatment presented here shows how the depth of field limitation can be understood as an envelope function which gradually attenuates the signal, starting well before the numerical depth of field is actually reached. A simple modification to the well-known back-projection reconstruction algorithm is described, called the defocus-gradient corrected back-projection, which computationally corrects for the contrast transfer function along a defocus gradient. Computer simulations demonstrate how the algorithm effectively eliminates the depth of field limitation. © 2000 Elsevier Science B.V. All rights reserved.

*Keywords:* Data processing; Image processing; Three-dimensional reconstruction

## 1. Introduction

Structure determination of spherical viruses by electron microscopy began with negatively stained bushy stunt virus to 28 Å resolution in 1970 [1]. Subsequent advances in microscope quality, specimen preparation, and data analysis have dramatically increased the resolution attainable, as evidenced by three recent studies of icosahedral viruses which reached resolutions adequate to reveal some secondary structure [2–4]. These successes have drawn attention to the prospect of atomic resolution and the remaining resolution limitations, which include the microscope depth of field [5].

Depth of field refers to the axial distance (distance parallel to the electron beam) within which specimen details will be similarly imaged to a specified resolution. An ideal imaging system would record specimen information at all spatial frequencies and all axial positions exactly. In the electron microscope, however, information is recorded according to an approximately sinusoidal contrast transfer function (CTF), which modulates the relative contributions of different spatial frequencies to the image. The CTF depends on several factors, including the electron wavelength and microscope defocus. Strictly speaking, the depth of field is defined as the defocus difference that causes a 180° phase shift in the CTF at a given resolution.

Images must be computationally corrected for the effects of the CTF before they can be used as faithful projections of the specimen in a three-dimensional reconstruction. If the diameter of a particle is sufficiently large that atoms near the top are

\*Corresponding author. Tel.: +1-650-723-6988; fax: +1-650-723-8464.

*E-mail address:* kornberg@stanford.edu (R.D. Kornberg).

imaged with a significantly different CTF than atoms near the bottom, however, not all of the information can be recovered from the projected image by correcting it for a single CTF. Because the CTF depends on both wavelength and defocus, there are two ways to overcome this limitation. The first way is to use a higher accelerating voltage (shorter wavelength). Microscopes operating at voltages up to 400 kV are now used routinely to image viruses. The second way of overcoming the depth of field limitation, discussed here, is to mathematically correct images for the variable CTF that governed the way information from each defocus level present in the specimen was recorded. One strategy for deconvoluting the effects of the CTF through the depth of a three-dimensional reconstruction, specifically directed to the study of large virus structures, has been proposed and encoded in the computer program COMET [6].

The purposes of this paper are threefold. The first is to describe how finite depth of field gradually attenuates signal with increasing resolution, and how it becomes a significant limiting factor long before the particle diameter actually exceeds the numerical depth of field. An expression is derived that gives the effective signal for an atom at a given radius from the center of a particle that would result from random particle projections, corrected for a defocus value appropriate for the particle's center, as has been done in all studies attempting a CTF correction to our knowledge. The second purpose is to propose a simple modification to the well-known back-projection algorithm, termed “defocus-gradient corrected back-projection”, which allows computational correction of the effects of depth of field. Finally, the resolution-enhancing effects of a depth-of-field correction are demonstrated by application of the defocus-gradient corrected back-projection to simulated data.

## 2. Signal attenuation due to depth of field

Given a particle frozen within a layer of vitreous ice in a random orientation, the probability that a particular atom at radius  $a$  will be found at height

$z$  above the central plane of the particle is proportional to the limit of the surface area of a sphere with radius  $a$  between heights  $(z - \Delta z/2)$  and  $(z + \Delta z/2)$ , as  $\Delta z$  approaches zero. The surface area of such a latitudinal strip is  $2\pi a \Delta z$  (see appendix), a remarkable result because it is independent of  $z$ , showing that any height  $z$  between  $-a$  and  $+a$  is equally likely. Thus, if the central plane of a particle being imaged lies at a defocus value  $z_0$ , for a particular atom at radius  $a$  from the center of the particle, any defocus value from  $(z_0 - a)$  to  $(z_0 + a)$  is equally likely.

Now considering any particular spatial frequency  $k$ , let us assume that the defocus value  $z_0$  is chosen exactly so that the CTF with defocus  $z_0$  has a maximum (value of 1.0) at that frequency. Then if a “perfect” (as opposed to a Wiener filter) CTF-correction of the image is done by simply dividing the image transform by the CTF appropriate for the defocus value  $z_0$ , no adjustment is made at frequency  $k$ . Thus, if an atom lies either above or below the central plane of the particle, where the defocus is no longer  $z_0$  and thus the CTF acting at that point is no longer at a maximum, the information about that atom at spatial frequency  $k$  will be diminished by the CTF, and the information will not be recovered during CTF correction (because only the CTF appropriate for the central plane is used). If the atom lies at height  $z$  with respect to the central plane, the ratio of the recovered signal to the true signal at frequency  $k$  is the value of the CTF with defocus  $z_0 + z$

$$\text{CTF}(k) = \sin \left[ 2\pi \left( -\frac{\lambda k^2 (z_0 + z)}{2} + \frac{\lambda^3 k^4 C_s}{4} \right) \right],$$

where  $\lambda$  is the electron wavelength,  $C_s$  is the coefficient of spherical aberration, and underfocus is represented by positive values of  $z_0 + z$ .

We now assume that there exists an ensemble of identical particles, each of which is frozen in random orientation with the central plane at defocus  $z_0$ . In the limit of an infinite number of particles, the ratio of the total signal recovered from a particular atom at frequency  $k$  to the true (full) signal present at frequency  $k$  will be the integral, over all possible atom elevations, of the CTF divided by the integral

of an ideal contrast transfer fraction whose value is always 1.

$$E(k, a) = \frac{\int_{z=-a}^{z=a} \text{CTF}(k) dz}{\int_{z=-a}^{z=a} dz}.$$

We label this result  $E(k, a)$ , as it is appropriately understood as an envelope function in reciprocal space that gradually attenuates the signal as a function of frequency and particle radius. Since the defocus  $z_0$  was chosen to give the CTF a value of 1.0 at frequency  $k$ ,

$$2\pi \left[ -\frac{\lambda k^2 z_0}{2} + \frac{\lambda^3 k^4 C_s}{4} \right] = \frac{\pi}{2},$$

so that

$$E(k, a) = \frac{1}{2a} \int_{z=-a}^{z=a} \cos(\pi \lambda k^2 z) dz,$$

$$E(k, a) = \text{sinc}(\pi \lambda k^2 a).$$

Representative curves were calculated for atoms at radii of 100–700 Å from the particle center, imaged with a 200 kV microscope (Fig. 1). These radii were chosen to represent the range of particle diameters currently encountered in single-particle analysis, noting that viruses with diameters as large as 1400 Å for the type 2 human adenovirus [7] and 1250 Å for the herpes simplex virus-1 [8] have already been studied. A voltage of 200 kV was chosen because microscopes operating at that voltage were used in three recent virus reconstructions that reached secondary structure resolution [2–4]. The result illustrates how the effective signal is attenuated long before the numerical depth of field is reached. For instance, although the depth of field of a 200 kV microscope at 5 Å resolution is 996 Å, approximately one-third of the effective signal from an atom on the surface of a particle with diameter 996 Å will be lost. Another example treats the possibility of using higher voltages alone to overcome depth of field limitations: if a particle has a radius of 700 Å (such as the type 2 human adenovirus), even if a 1 MeV microscope is used, half the signal at atomic ( $\sim 3$  Å) resolution will still be lost (Table 1). While microscopes using voltages higher than 1 MeV are available, none are currently equipped with the highly coherent, field emission electron guns so important for high-resolution studies.

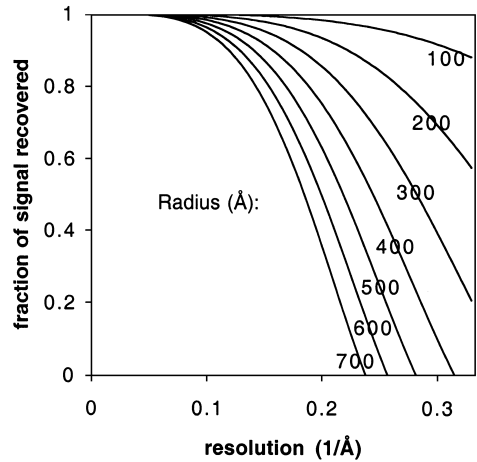


Fig. 1. Signal decay as a function of resolution and particle radius. The fraction of the ideal signal that is actually recovered after standard (single valued) CTF correction is shown as a function of resolution for various particle radii. The curves are sinc functions, as derived in the text, and are appropriate for a 200 kV microscope.

This treatment illustrates the extent to which the phenomenon of depth of field already limits the resolution of current reconstructions, and further emphasizes the requirement for a method to computationally correct this loss before atomic resolution reconstructions of large viruses can be expected. The same conclusion has been reached through an analysis of phase errors [5], and related derivations of the sinc function shown above can be found elsewhere [9,10].

### 3. Defocus-gradient corrected back-projection

To computationally correct for the limitations of depth of field, we propose a simple modification to the well-known back-projection algorithm commonly used in three-dimensional reconstruction from electron micrographs [11]. The essence of the modification is to perform multiple CTF corrections, appropriate for different heights within the particle, on each projection image used in the back-projection. The back-projection body is then divided into layers, and the information from an image is back-projected into each layer of the

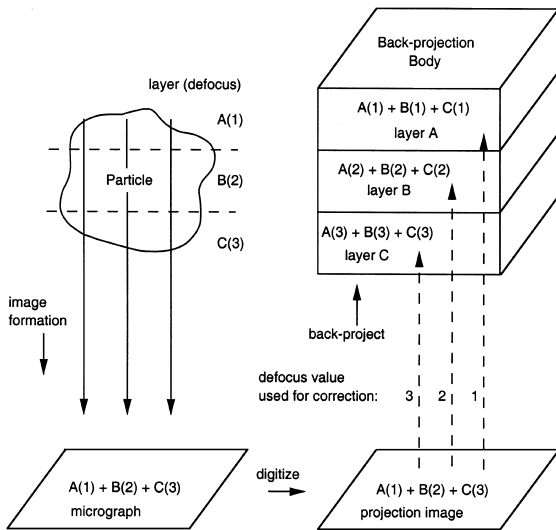


Fig. 2. Schematic explanation of the defocus-gradient corrected back-projection algorithm. A particle is shown on the left, divided into three hypothetical layers A–C, which are each imaged according to a CTF determined by the defocus value (numbered 1, 2, or 3 in parenthesis) appropriate for that height within the specimen. During image formation, the information from each layer is projected and recorded onto the micrograph. The defocus-gradient corrected back-projection proceeds by duplicating the digitized projection image several times (three would be necessary for the procedure as shown), and performing a CTF correction on each copy with defocus values appropriate for different levels within the particle. Then as each voxel within the back-projection body is filled, data from the correspondingly corrected version of the image is used. Projections from many different angles must be included for the particle structure to emerge.

reconstruction using the appropriately corrected version of the image.

The defocus-gradient corrected back-projection is schematically depicted in Fig. 2. On the left is a particle and its projection pattern recorded as an electron micrograph. The particle has been arbitrarily divided into three layers, namely A–C, to illustrate how information from each layer is recorded and recovered. Each layer lies at a different defocus, represented by the number in parenthesis (1, 2, or 3). During image formation, the information from each level in the structure is modulated by the defocus-dependent CTF and superimposed in the micrograph. The back-projection procedure can be thought of as filling each voxel in the back-projection body with the actual density that existed

in that position in the real structure plus all the projected density above and below it, which can be understood as a signal plus noise. The emergence of the correct structure in the model occurs through the inclusion of multiple views, which serve to reinforce the signal at each voxel but not the noise. If the projection image is CTF corrected appropriately for only one layer within the particle, the back-projection body for that particular layer will be filled with some valid signal. All other layers, however, will be filled with only noise, since the specimen details recorded from those layers are lost in the mis-corrected CTF.

In the defocus-gradient corrected back-projection, shown on the right side of Fig. 2, the projection image is CTF-corrected independently three times, once for each of the three layers, using defocus values appropriate for that layer. Then the three layers of the back-projection are filled using data from the correspondingly corrected version of the image. Thus the signal going into each layer of the back-projection body will be appropriately CTF-corrected, while the noise, which arises from the other layers, will not. For instance in layer C in the back-projection body, the signal comes from layer C in the particle, and is appropriately CTF-corrected with defocus value  $\neq 3$ . The noise comes from particle layers A and B, whose irrelevant information is corrupted by CTF correction with the inappropriate defocus value  $\neq 3$ . As the number of layers independently corrected increases, the structure should emerge more and more quickly.

In the context of the Ewald sphere construction, we note that the curvature of the Ewald sphere is constant for a given electron wavelength, but that the extent to which that curvature limits resolution depends on specimen thickness. Thus while the treatment of a thick specimen as a stack of thin layers does not diminish the curvature of the Ewald sphere, it can reduce the effects of that curvature to any degree desired.

#### 4. Demonstration of the resolution-enhancing effects of the defocus-gradient corrected back-projection

The effectiveness of the defocus-gradient corrected back-projection was tested with different

numbers of independently corrected layers using simulated images of a biological particle. The resolution of the back-projection was followed as a function of the number of images included. Atomic coordinates for the model particle were obtained from file 1vol.mmol in the PDB database [12]. This particle has a mass of about 50 kDa and a diameter of 90 Å, and was chosen randomly from many potential particles with similar size and asymmetry. The small size reduced data storage and time demands.

Images were simulated by first rotating the particle by random rotation angles, followed by bilinear interpolation of the atomic masses in the particle onto a stack of 49 parallel planes of dimension  $330 \text{ Å} \times 330 \text{ Å}$  with  $1.0 \text{ Å}$  grid spacing, each  $1.928 \text{ Å}$  apart along the  $z$ -axis. These planes were then Fourier transformed, and all the amplitudes were adjusted by an appropriate full CTF, including both amplitude and phase contrast, with the addition of a defocus-exaggeration factor  $X$  multiplying the defocus  $z$  to artificially exaggerate the effects of depth of field

$$\gamma = 2\pi \left( -\frac{\lambda k^2 X z}{2} + \frac{\lambda^3 k^4 C_s}{4} \right),$$

$$\text{CTF}_{\text{full}}(k) = (1 - P)\sin(\gamma) - P \cos(\gamma),$$

where the fraction of amplitude contrast ( $P$ ) was 0.08, the coefficient of spherical aberration  $C_s$  was  $2.0 \text{ mm}$ , and the electron wavelength  $\lambda$  was  $0.0370 \text{ Å}$  (appropriate for 100 kV). The defocus-exaggeration factor  $X$  was chosen as the diameter of a large virus ( $1400 \text{ Å}$ ) divided by the diameter of the simulation particle ( $90 \text{ Å}$ ), so that the same magnitude of the depth of field problems faced in the reconstruction of such a large virus could be manifest through a much smaller particle that facilitated the simulation. The defocus value of the central plane in each particle was chosen from a Gaussian distribution so that after multiplication by the defocus-exaggeration factor, the corresponding defocus range would have a mean of  $1.5 \text{ }\mu\text{m}$  underfocus and standard deviation of  $0.5 \text{ }\mu\text{m}$ . The defocus value of each non-central plane was adjusted appropriately by adding or subtracting  $1.982 \text{ Å}$  increments (a defocus change equivalent to

$30 \text{ Å}$  after correction for the exaggeration factor). After imposition of the corresponding full CTF to each projection plane, the stack was superposed by vector addition in reciprocal space, and the superposition was inverse Fourier-transformed back to real space to become the simulated particle image.

Three-dimensional reconstruction from projected images was done with a weighted back-projection method closely following the algorithms given by Radermacher [11] with bilinear interpolation of densities, with the defocus-gradient corrected back-projection modifications as described above and depicted in Fig. 2. CTF corrections were performed by multiplying image transforms by the Wiener filter appropriate for each defocus value, which for noiseless images such as these, is equivalent to simply dividing by the CTF. Back-projection bodies and reconstructions had sidelengths of  $182 \text{ Å}$ , with  $1.0 \text{ Å}$  spacings.

After each set of 10 new images had been added to the back-projection body, the resolution of the model was assessed by comparison to an ideal reconstruction as follows. First, a model of the structure was generated by deconvolving the back-projection body with the point spread function dictated by the set of projection angles included to that point. A real space mask was applied to de-emphasize features in the model not associated with the particle. The mask was spherically symmetric, having a value of 1.0 out to a radius of  $50 \text{ Å}$ , and then falling off with a Gaussian shape so that the value at  $70 \text{ Å}$  was  $e^{-1}$ . The mask did not introduce significant correlation between models at frequencies higher than  $\frac{1}{2} \text{ Å}^{-1}$ . Next the masked model was matched in mean value and variance to an ideal reconstruction calculated by trilinear interpolation of the atomic masses onto a three-dimensional lattice. An amplitude-weighted phase difference between the masked model and the ideal reconstruction was computed for shells in Fourier space (using amplitudes from the ideal reconstruction), and the resolution of the model was defined as the highest resolution shell with a difference less than  $45^\circ$ .

Fig. 3 shows the resolution as a function of number of images included for simulations using the defocus-gradient corrected back-projection algorithm with various correction-layer thicknesses

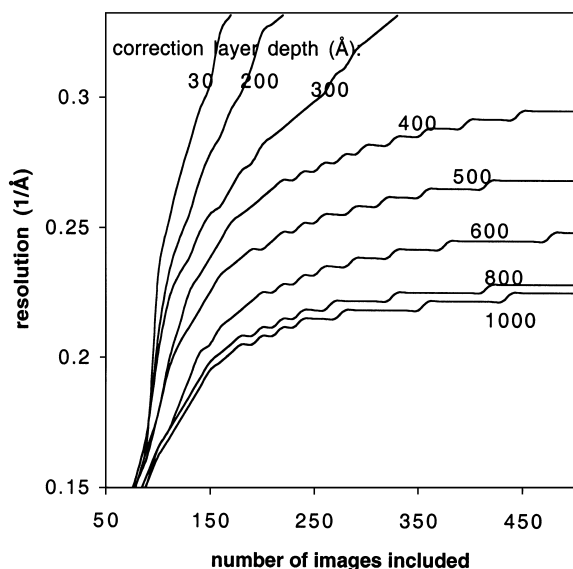


Fig. 3. Demonstration of the defocus-gradient corrected back-projection. The resolutions of models calculated using the defocus-gradient corrected back-projection algorithm with various layer thicknesses are shown as a function of the number of images included.

(adjusted for the defocus exaggeration factor). The reconstructions asymptotically approach the resolution to which the uncorrected depth of field becomes limiting. For example, when the correction is performed with 600 Å thick layers, the reconstruction asymptotically approaches 4 Å resolution, just beyond the resolution (4.29 Å) at which depth of field causes loss of half the signal from a particle with similar diameter (see Table 1). Back-projections done with correction layers more than 1000 Å thick, or with a single CTF correction appropriate for the central plane of the particle, asymptotically reached resolutions slightly worse than the reconstruction with the 1000 Å correction layer (data not shown). The curve representing 30 Å correction layers demonstrates that if thin reconstruction layers are used, the application of the defocus-gradient corrected back-projection effectively removes the depth of field limitation, allowing atomic resolution reconstructions of even thick particles (1400 Å) with common (100 kV) microscopes.

Table 1

Resolutions (in Å) at which half the potential signal is lost because of depth of field limitations for various particle radii and microscope voltage

Radius (Å)	100 (kV)	200 (kV)	300 (kV)	400 (kV)	1 (MV)
100	2.48	2.04	1.81	1.65	1.20
300	4.29	3.53	3.13	2.86	2.08
500	5.54	4.56	4.04	3.69	2.69
700	6.55	5.39	4.78	4.36	3.18

## 5. Conclusions

Despite the introduction of intermediate voltage microscopes, the depth of field in transmission electron microscopy is still a significant limitation in the three-dimensional reconstruction of large particles at near atomic resolution. While the problem is greatest for the large viruses commonly studied today, it is shown here that depth of field limitations can significantly reduce the highest resolution signals from smaller particles as well (see Table 1). An algorithm, termed the defocus-gradient corrected back-projection, is described and demonstrated to effectively remove the depth of field limitation.

For the particular case of large icosahedral viruses, there are disadvantages to the real space-based reconstruction technique proposed. The entire volume is typically stored and reconstructed at once, rather than just the unique coefficients in Fourier space that determine the structure. While possible with currently available hardware, this would nevertheless require special equipment. Consider reconstructing the type 2 human adenovirus (1400 Å diameter) to atomic resolution. A back-projection body that would comfortably accommodate the virus could be around  $1400^3$  pixels (1.5 times the dimension of the particle with 1.5 Å/pixel), and require on the order of 5 gigabytes of memory. Furthermore, because Fourier space-based techniques can more efficiently average data from large numbers of projections, the back-projection method may be comparatively slow. For these and other reasons, icosahedral virus studies are now done using Fourier-Bessel reconstructions.

It is unclear, however, whether a similar defocus-gradient correction could be applied in Fourier space because a single central section in reciprocal space (which contains the information from each projection image) cannot be corrected for multiple defocus values simultaneously. It is only when the structure is considered in real space that the superposition of information from the various layers of the specimen can be selectively corrected with appropriate defocus values. Perhaps real space reconstruction algorithms for particles with high degrees of symmetry can be modified to store only a single asymmetric unit and incorporate the information from each of the symmetrically related views present in a particle image successively.

The defocus-gradient corrected back-projection presented here requires no initial model for subsequent refinement, and thus may be particularly useful to introduce the CTF corrections immediately into models generated from raw data. Because it is a simple modification to the commonly used and familiar back-projection algorithm, it can be conveniently introduced into established processing strategies.

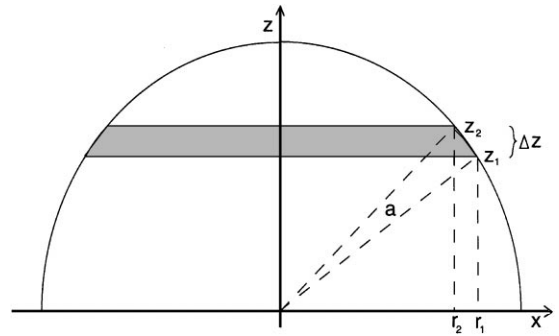
## Acknowledgements

G.J.J. was supported by a Medical Scientist Training Program grant (GM07365) provided by the National Institute of General Medical Science at the National Institutes of Health. This research was supported by National Institutes of Health Grant AI21144 to R.D.K.

## Appendix A. The surface area of a latitudinal strip around a sphere

The surface area  $A$  of a function  $z = f(x, y)$  is given as

$$A = \iint_S \sqrt{f_x^2 + f_y^2 + 1} \, dS,$$



where  $S$  is the surface of integration,  $f_x$  and  $f_y$  are the first partial derivatives of  $f$  with respect to  $x$  and  $y$ , respectively, and  $dS$  is a differential unit of surface area. For a sphere of radius  $a$ ,

$$f(x, y) = z = \sqrt{a^2 - x^2 - y^2}$$

so that

$$f_x^2 = \frac{x^2}{a^2 - x^2 - y^2} \quad \text{and} \quad f_y^2 = \frac{y^2}{a^2 - x^2 - y^2}$$

Thus

$$A = \iint_S \frac{a}{\sqrt{a^2 - x^2 - y^2}} \, dS,$$

which in polar coordinates becomes

$$A = \int_{\theta=0}^{\theta=2\pi} \int_{r=r_1}^{r=r_2} \frac{a}{\sqrt{a^2 - r^2}} r \, dr \, d\theta.$$

After integration,

$$A = 2\pi a [\sqrt{a^2 - r_2^2} - \sqrt{a^2 - r_1^2}].$$

Converting back to Cartesian coordinates (using  $r_i^2 = a^2 - z_i^2$ ) yields

$$A = 2\pi a(z_2 - z_1) = 2\pi a \Delta z.$$

## References

- [1] R.A. Crowther, L.A. Amos, J.T. Finch, D.J. De Rosier, A. Klug, *Nature* 226 (1970) 421.
- [2] B. Böttcher, S.A. Wynne, R.A. Crowther, *Nature* 386 (1997) 88.

- [3] J.F. Conway, N. Cheng, A. Zlotnick, P.T. Wingfield, S.J. Stahl, A.C. Steven, *Nature* 386 (1997) 91.
- [4] B.L. Trus, R.B.S. Roden, H.L. Greenstone, M. Vrhel, J.T. Schiler, F.P. Booy, *Nat. Struct. Biol.* 4 (1997) 413.
- [5] E.J. Mancini, F. de Haas, S.D. Fuller, *Structure* 15 (1997) 741.
- [6] U. Skoglund, L. Öfverstedt, *J. Struct. Biol.* 117 (1996) 173.
- [7] P.L. Stewart, S.D. Fuller, R.M. Burnett, *EMBO J.* 12 (1993) 2589.
- [8] W.W. Newcomb, F.L. Homa, D.R. Thomsen, F.P. Booy, B.L. Trus, A.C. Steven, J.V. Spencer, J.C. Brown, *J. Mol. Biol.* 263 (1996) 432.
- [9] R.H. Wade, *Ultramicroscopy* 46 (1992) 145.
- [10] E. Zeitler, in: L. Marton (Ed.), *Advances in Electronics and Electron Physics*, Vol. 25, Academic Press, London, 1968, p. 227.
- [11] M. Radermacher, in: J. Frank (Ed.), *Electron Tomography: Three-Dimensional Imaging with the Transmission Electron Microscope*, Plenum Press, New York, 1992, p. 91.
- [12] D.B. Nikolov, H. Chen, E.D. Halay, A.A. Usheva, K. Hisatake, D.K. Lee, R.G. Roeder, S.K. Burley, *Nature* 377 (1995) 119.